First-order reversal curve diagram analysis of a perpendicular nickel nanopillar array

C. R. Pike,[1] C. A. Ross,[2] R. T. Scalettar,[1] and G. Zimanyi[1]
[1]*Physics Department, University of California, Davis, California 95616, USA*
[2]*Department of Materials Science and Engineering, Massachusetts Institute of Technology, Cambridge, Massachusetts 02139, USA*
(Received 5 March 2004; revised manuscript received 1 November 2004; published 12 April 2005)

We apply a first-order reversal curve (FORC) diagram analysis to a perpendicular nickel nanopillar array. We find that the FORC diagram signature of this system consists of a two-branch "wishbone" structure. Two distinct negative regions are also observed, along with a prominent reversible ridge. The objective of this paper is to find a qualitative physical understanding or interpretation of these features. To accomplish this, we employ an interacting hysteron model. We find that a collection of symmetric hysterons with distributed coercivities and antiparallel mean field can account for the wishbone signature and one of the negative regions. By employing curvilinear hysterons, we can account for the reversible ridge and the other of the negative regions. Through a comparison of modeling and experimental work, we obtain a quantitative estimate of the dipolar interaction strength.

DOI: 10.1103/PhysRevB.71.134407 PACS number(s): 75.50.Ss, 75.60.Ej, 75.75.+a

I. INTRODUCTION

Patterned arrays of single domain nanomagnets have been proposed as candidates for high-density perpendicular magnetic recording media.[1] An understanding of the magnetic properties of the individual particles, as well as the nature of the interactions between them, has been the goal of recent experimental and theoretical studies.[2–7]

First-order reversal curve (FORC) diagrams[8] may provide a useful tool for the characterization of patterned perpendicular magnetic media. FORC diagrams are based on the procedure described by Mayergoyz for identifying the Preisach distribution of a classical Preisach system.[9] In a FORC diagram analysis we treat this same procedure as simply a type of measurement, which can be performed on any magnetic system regardless of whether that system is consistent with the classical Preisach model. On a FORC diagram, each magnetic system exhibits a "signature" which contains detailed information about that system's magnetic properties.[8,10–16]

Here we look at the FORC diagram signature of a perpendicular nickel nanopillar array. Our objective is to develop a qualitative physical interpretation of this signature and its features. We are also interested in what physical quantities can be extracted from the FORC distribution.

This paper is organized as follows: After a review of FORC diagrams, we report measurements of the FORC diagram signature of a perpendicular nickel nanopillar array. We then show that a simple hysteron model with distributed coercivities and a negative (antiparallel) mean interaction field can account for the basic qualitative features of this signature. We next show that some of the finer features of this signature can be accounted for by replacing the mean field with a "dipolar" interaction field, and by introducing disorder into the interactions. Finally, we augment our model by incorporating reversible magnetization through the use of curvilinear hysterons. By fitting our model to experimental data, we obtain a quantitative measure of the interaction strength in our sample.

II. REVIEW OF FORC DIAGRAMS

A FORC diagram is generated from a collection of first-order reversal curves (FORCs), such as the one illustrated in Fig. 1. The generation of a FORC is preceded by the saturation of a system in a positive applied field. The field is then lowered to a reversal field H_r, and a FORC is the magnetization curve that results when the applied field is increased back to saturation.[9] The magnetization at the applied field H_a on the FORC with reversal field H_r is denoted by $M(H_r,H_a)$. The FORC distribution is defined as the mixed second derivative:

$$\rho(H_r,H_a) = -\frac{1}{2}\frac{\partial^2 M(H_r,H_a)}{\partial H_r \partial H_a}. \tag{1}$$

We employ FORC datasets which have a uniform field spacing H_{sp} in both the applied and reversal fields. In order to perform the second derivative in Eq. (1) on a dataset, we employ a polynomial fit on a local neighborhood consisting of a square with five data points on each side.[8] For the purposes of plotting a FORC distribution, it is convenient to change coordinates from $\{H_a,H_r\}$ to $\{H_c=(H_a-H_r)/2, H_b=(H_a+H_r)/2\}$.

Let us consider the FORC distribution in the simple case of the "hysteron" s shown in Fig. 2. A hysteron is a mathematical construction which generates a square hysteresis loop in an applied field H. The half-width and offset of s are referred to as its coercivity and bias, denoted by h_c and h_b, respectively. A hysteron with zero bias is referred to as a symmetric hysteron. The value of s depends on the applied field history in the following way: If we let the applied field begin at $H=\infty$, then s will start at +1; s will switch to −1 whenever H falls below $(-h_c+h_b)$, and will switch back to +1 whenever H rises above (h_c+h_b). The FORC distribution of the hysteron s is simply a point Dirac δ function at the coordinates $H_c=h_c$ and $H_b=h_b$. This is the motivation for referring to these as the coercivity and bias axis. Given an assemblage of symmetric hysterons with a distribution of coercivities $f(h_c)$, one will obtain a FORC distribution of the

 ©2005 The American Physical Society

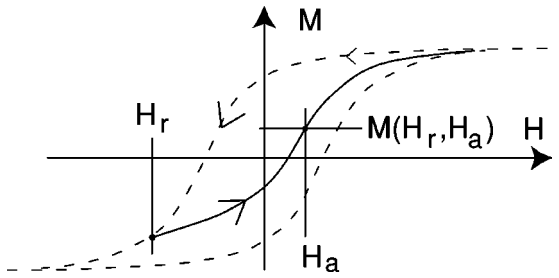

FIG. 1. A first-order reversal curve (FORC) is acquired after saturating the sample in a positive applied field. The applied field is lowered to a reversal field H_r. A FORC is the magnetization curve that results when the applied field H_a is increased back to saturation. The magnetization at the applied field H_a on a FORC with reversal field H_r is denoted by $M(H_a,H_r)$.

form $\rho(H_c,H_b)=\delta(H_b)f(h_c)$, which is a delta function "ridge" on the $H_b=0$ axis.

In general, the magnetic response of a material is a convolution of reversible and irreversible magnetizations. As it has just been described, a FORC distribution does not capture the contribution of a reversible magnetization. However, it has been shown that a reversible magnetization can be captured be means of extended FORCs.[17] An extended FORC is defined as

$$M^{\text{ext}}(H_a,H_r) \equiv \begin{cases} M(H_a,H_r) & \text{if } H_a \geqslant H_r, \\ M(H_r,H_r) & \text{if } H_a < H_r \end{cases} . \qquad (2)$$

When the FORC distribution is calculated with the extended FORCs in Eq. (2), then one obtains a "reversible ridge" on the $H_c=0$ axis which is given by

$$\rho(H_c=0,H_b)=\frac{1}{2}\delta(H_c)\lim_{H_a\to H_r^+}\left.\frac{\partial M(H_a,H_r)}{\partial H_a}\right|_{H_r=H_b}. \qquad (3)$$

The derivative in Eq. (3) is the slope of the FORC with reversal field $H_r=H_b$ where that FORC is joined to the major hysteresis loop. This is equivalent to the reversible susceptibility on the descending major hysteresis loop at applied field H_b. The FORC distribution with the extended FORCs in Eq. (2) captures the entire magnetic response, so that the total weight of the distribution equals the saturation magnetization.[17]

If a system contains a reversible magnetization of the simple form $M_{rev}(H)$, then this reversible magnetization will give rise to a delta function ridge in the FORC distribution of the form

$$\rho(H_c,H_b)=\frac{1}{2}\delta(H_c)\frac{dM_{rev}(H_b)}{dH_b}. \qquad (4)$$

More generally, however, the reversible magnetization will be coupled to the irreversible magnetization. This coupling implies that the "reversible magnetization" may not be globally reversible. As a result, the "reversible magnetization" may actually contribute features to the FORC distribution which are located off the $H_c=0$ axis. This effect will be demonstrated by the particulate magnetic media example we consider next.

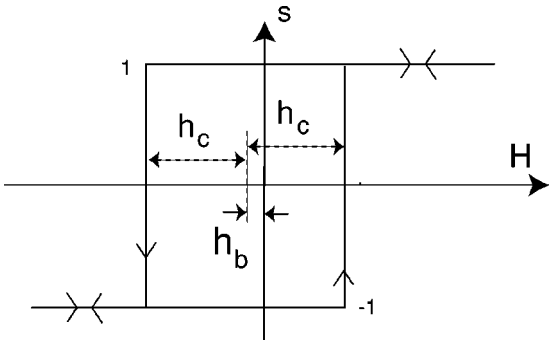

FIG. 2. A hysteron s with coercivity h_c and bias h_b. A hysteron with zero bias is said to be symmetric.

In this paper, we will be looking at a magnetic media which is a candidate for perpendicular magnetic recording. Before doing so, it may be worthwhile to consider the FORC distribution of a magnetic media used in the older and simpler longitudinal recording technology. The sample we have chosen is a Sony High Density floppy disk, which contains a dispersion of fine particles in a polymer film. We use the case of this floppy disk sample to illustrate some important ideas in FORC diagram analysis which will prove useful in the study of our nanopillar array sample.

In Fig. 3(a) we show the FORC distribution of the Sony disk sample. The measurements were done in the plane of the disk. The magnetization of the FORCs were normalized by the saturation magnetization before calculating this distribution. A legend for the contour shadings is shown above the diagram. Max denotes the value of the FORC distribution at its "irreversible" peak located at about $H_c=90$ mT. Note that ρ goes to zero at the right-hand boundary of the diagram. The shading at this boundary corresponds to $\rho\approx 0$; lighter shadings represent negative regions of ρ. The "reversible" ridge in Fig. 3(a) appears as a dark vertical stripe at $H_c=0$. For a better look at this ridge, we plot a horizontal cross-section at $H_b=-5$ mT in (b) and a vertical cross-section through $H_c=0$ in (c).

If temperature and interaction effects are ignored, then this particulate system can be treated to a rough approximation as a collection of square hysterons. In this simple treatment, we would expect the FORC distribution due to the square hystersons to consist of a sharply peaked horizontal ridge on the $H_b=0$ axis. But in Fig. 3(a) we can see that the "irreversible" peak at about $H_c=90$ mT actually has considerable vertical spread (i.e., spread in the bias distribution). It has been shown experimentally that this spread increases with an increasing concentration of particles.[8–18] This suggests that the spread in the bias distribution can be attributed primarily to dipole interactions, and that the amount of spread can be used as a measure of the interaction strength in this type of media.

The reversible magnetization can be incorporated into this simple theoretical treatment by adding a reversible magnetization of the simple form $M_{rev}(H)$. In this form, the reversible and irreversible magnetizations are decoupled. But in a more realistic treatment, the reversible and irreversible magnetizations would be coupled. For example, if we treat these particles as Stoner-Wholfarth-type particles, then the slope

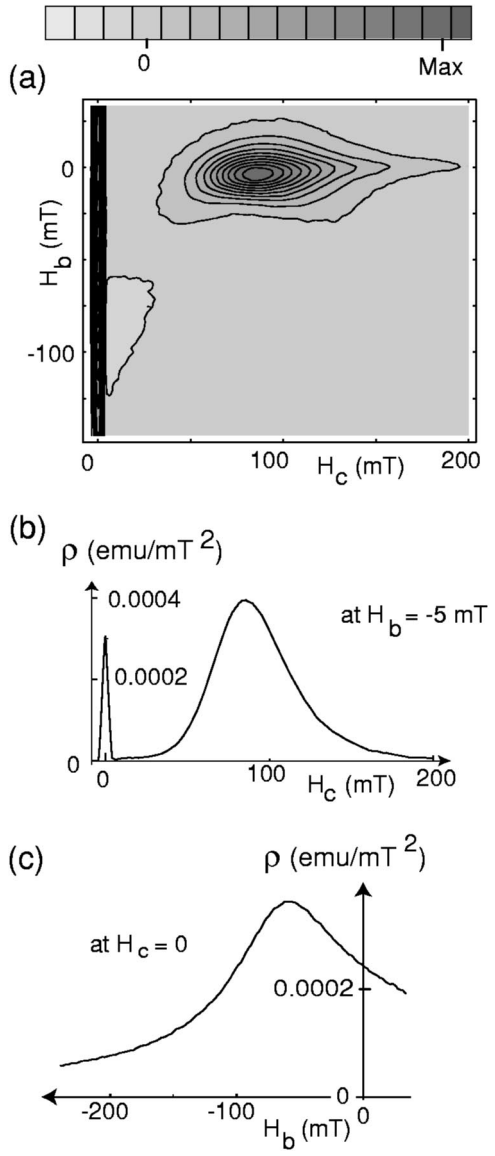

FIG. 3. (a) A FORC diagram for Sony high density floppy disk sample. In the legend for the contour shading, Max denotes the value of the FORC distribution at its "irreversible" peak located at about H_c=90 mT. A prominent reversible ridge appears on the H_c =0. Note that the high density of vertical contour lines near the H_c=0 axis makes the shading there appear darker than it actually is. A negative region occurs adjacent to the reversible ridge at about H_b=−85 mT. The shape of the reversible ridge is conveyed by the two cross sections in (b) and (c). In (b) we plot a horizontal cross section passing though the irreversible peak at H_b=−5 mT. In (c) we plot a vertical cross section through the reversible ridge at H_c=0.

(or susceptibility) of their hysteresis loops near the negative switching field is greater on the top branch than on the bottom (except in the specific case of a particle whose easy axis is aligned with the applied field, in which case the hysteresis loop is just a square loop). This difference in slope between the top and bottom branches implies that the reversible and irreversible components are coupled, and it leads directly to the negative valley located in the lower part of Fig. 3(a).[17,20]

As described later, we will find a similar negative valley in the FORC distribution of our nanopillar array.

A more detailed analysis of the FORC distribution in Fig. 3(a) shows that the spread (i.e., standard deviation) in bias is actually greatest at low H_c and vanishes toward high H_c, resulting in the high coercivity "tail" seen in Fig. 3(a).[19] This behavior can be attributed to "completion symmetry" which can be described in the following manner: Let us suppose that in some neighborhood of this particulate media, there is one particle which is always the last to switch into the direction of the applied field. It can be said that this particle "completes" the reversal of its local neighborhood. Let us refer to this particle as a "completion particle." The interaction field experienced by a completion particle when it switches positive is approximately equal and opposite to the interaction field it experiences when it switches negative. Because of this symmetry, a completion particle behaves as if it has little or no bias. The decreasing bias spread toward large H_c in Fig. 3(a) has been attributed to particles which behave like completion particles. As one proceeds toward high H_c, the completion symmetry just described forces the distribution's bias to approach zero.[19]

The same completion symmetry has been found in the Edwards-Anderson spin glass (EASG).[14] The EASG is an Ising model with nearest-neighbor random interactions, distributed around zero, thus having an equal number of ferromagnetic and antiferromagnetic bonds. In the FORC distribution for the EASG, a sharp ridge has been found on the H_c axis (i.e., zero bias) at high coercivity. This ridge is due to particles which consistently are, the last in their local neighborhood to switch into the direction of the applied field, i.e., completion particles. In the case of the particulate media discussed above, since the interactions are long range dipolar, completion symmetry is not an exact relationship. As a result, its effect is somewhat subtle. By contrast, since interactions are short range in the EASG model, completion symmetry can be exact. As a result, the ridge on the H_c axis of the Edward-Anderson spin glass FORC distribution is quite dramatic.[14]

Completion symmetry is a common theme in many FORC distributions. As described below, we will find the effect of completion symmetry in the FORC distribution of our nanopillar array.

III. EXPERIMENT

The sample in this study was an array of Ni pillars with diameter 92 nm, height 250 nm, and period 200 nm. The Ni is polycrystalline with a grain size of 10 to 20 nm. A scanning electron micrograph is shown in Fig. 4. The sample was made by interference lithography and electrodeposition, in a process described previously,[7] and was made simultaneously with the sample shown in Fig. 1(b) of Ref. 7. According to magnetic force microscopy, each pillar constitutes a magnetic single domain with easy axis parallel to the long axis, i.e., perpendicular to the plane of the substrate.

A set of 140 FORCs (H_{sp}=1.5 mT) was measured with a Princeton Measurements Alternating Field Magnetometer as shown in Fig. 5(a). Measurements were done perpendicular

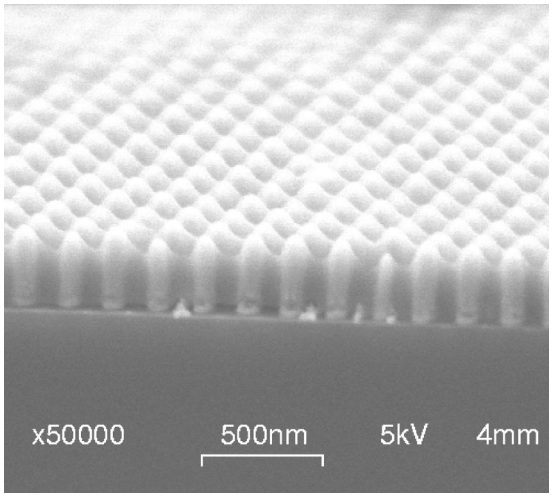

FIG. 4. Scanning electron micrograph of pillar sample.

to the substrate. The magnetization was normalized by the saturation magnetization. The FORC distribution generated from this data is shown in Fig. 5(b). Again, Max denotes the value of ρ at the "irreversible peak," which is located in the case at about $H_c = 23$ mT, $H_b = 20$ mT. A large reversible ridge can be seen on the $H_c = 0$ axis. The most prominent feature of the FORC distribution, aside from the reversible ridge, is a two branch "wishbone" structure. The vertical cross-section through this ridge is shown in Fig. 5(c). Two negative "valleys" can be also be seen in Fig. 5(b): one at high coercivity just below the $H_b = 0$ axis, and another adjacent to the reversible ridge.

In the following sections we develop a qualitative understanding of the physical mechanisms which give rise to the features of this measured FORC signature.

IV. MEAN FIELD MODELING

We next show that the wishbone structure of the FORC signature in Fig. 5(b) can be qualitatively accounted for using a interacting hysteron model with a negative (antiparallel) mean field and distributed coercivities. Let us begin with a collection of N square and symmetric (zero bias) hysterons. The state of the ith hysteron is denoted by s_i, which can take values of ± 1. The pillars in this array do not have a perfectly uniform shape and size; they also likely contain a high density of defects, vacancies, and inhomogeneities. Therefore a distribution of coercivities is expected. The coercivity of the ith hysteron is denoted by h_i^c. The distribution of coercivities is denoted by $f(h_c)$. The total normalized magnetization of the system is given by

$$M = \sum s_i / N. \tag{5}$$

Since the magnetization of the nickel pillars is dominantly oriented perpendicular to the plane of the substrate, then the dipolar interaction is antiparallel to the direction of the magnetization. In this section we will represent this interaction by a mean interaction field written as

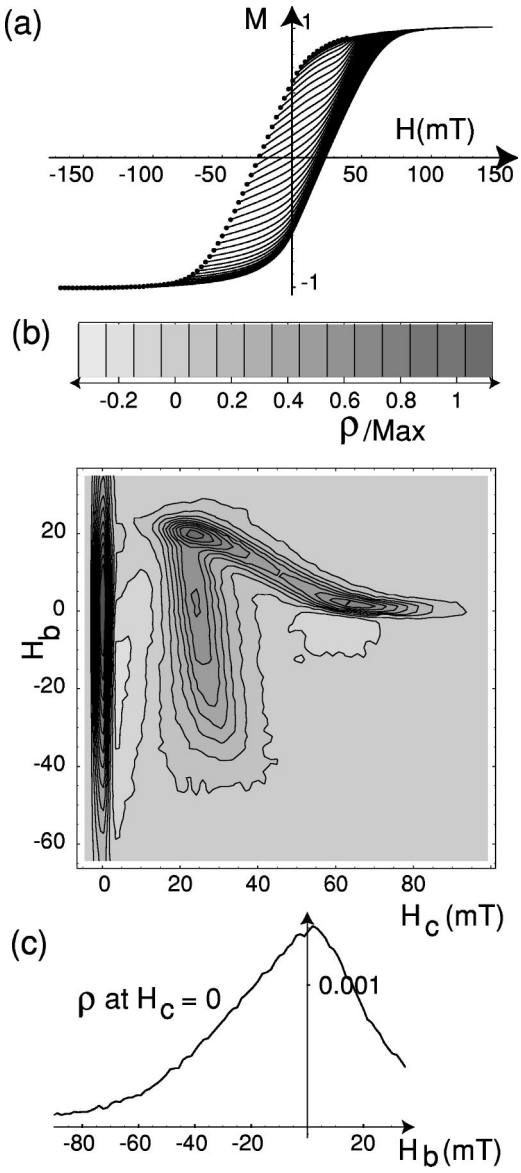

FIG. 5. (a) The first-order reversal curve (FORC) data for nickel pillar sample. To make it easier for the eye to resolve individual curves, only 70 of the 140 measured FORCs are shown. (b) The FORC distribution generated from this data. Max denotes the value of the distribution at the "irreversible" peak located at about $H_c = 23$ mT, $H_b = 20$ mT. On the $H_c = 0$ vertical axis is a sharply peak ridge due to reversible magnetization.(c) The vertical cross section through the "reversible" ridge at $H_c = 0$ as a function of H_b.

$$H^{int} = -JM, \tag{6}$$

where J is the magnitude of the total interaction field seen by the hysterons in the saturated state. The total field is the sum of the externally applied field H and H^{int}. In our algorithm for calculating FORCs, the applied field H was initially given a large value and the s_i were all set to +1. Then H is lowered in small "field steps". To obtain robust numerical results with interacting systems, the size of the field steps should be much smaller than the width of the coercivity distribution. Note that a "field step" is distinct from a "field

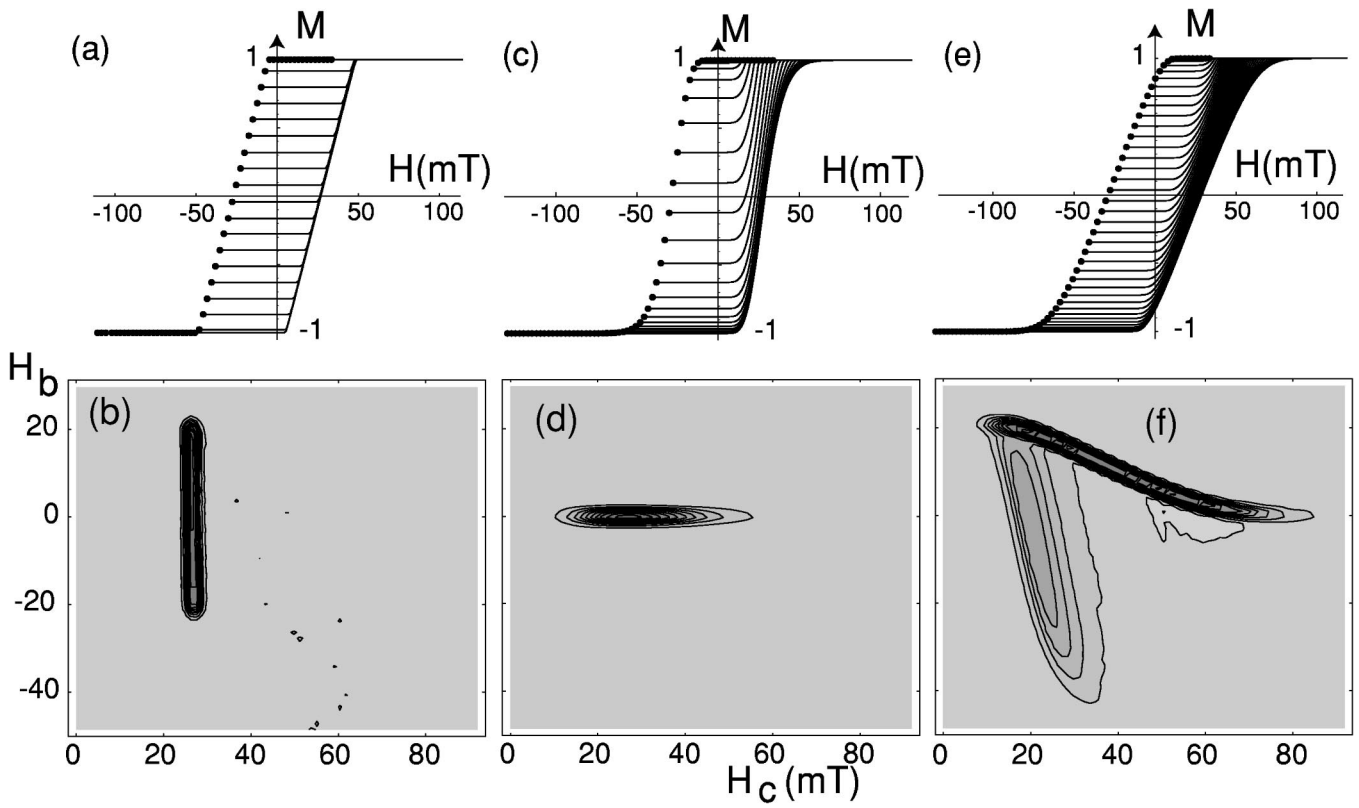

FIG. 6. The FORCs and the FORC distribution of a collection of hysterons with mean field interactions: (a) and (b) a narrow Gaussian coercivity distribution and $J=21.1$ mT; a broader Gamma distribution with $J=0$ [(c) and (d)] and with $J=21.1$ mT [(e) and (f)]. Only 70 of the 140 calculated FORCs are shown in (a), (c), and (e). Many of these FORCs coincide and cannot be distinguished in this plot.

spacing". "Field spacing" refers to the spacing between the data points in a FORC dataset. Each field spacing is divided into N_{st} field steps.

After each field step, the values of the s_i are updated in this fashion: If $s_i=1$ and

$$H^{int}+H<-h_i^c, \tag{7}$$

then s_i is updated to -1; if $s_i=-1$ and

$$h_i^c<H^{int}+H, \tag{8}$$

then s_i is updated to $+1$. In our algorithm, the value of H^{int} used in this updating is obtained from the state of the system at the previous field step. In this manner, the descending hysteresis loop is calculated down to a reversal field H_r. To obtain a FORC, we begin incrementing the field starting from this reversal field and update the hysterons in a similar fashion.

It is instructive to first look at this mean field model in the case of a very narrow coercivity distribution. We let $f(h_c)$ be a Gaussian with mean 27 mT and standard deviation 0.027 mT, and we let $J=21.1$ mT. In all the numerical calculations of this paper, we let $N=160{,}000$, $N_{\mathrm{st}}=150$, and we calculate 140 FORCs for each diagram. The numerically calculated FORCs ($H_{\mathrm{sp}}=1.3$) and FORC distribution are shown in Figs. 6(a) and 6(b). The FORC distribution shows a narrow and vertically elongated ridge. In the Appendix we give an analytical derivation of this same result. Next, we suggest a qualitative explanation for this vertical ridge.

Assume that the hysterons are ordered with ascending h_c, so that $h_{i+1}^c>h_i^c$. Then the lowest coercivity in the collection is equal to h_1^c and the highest coercivity is denoted by h_N^c. As the reversal field is lowered from saturation, the first hysteron to switch negative is $i=1$, and it will switch down at $H_r=-h_1^c+J$ (since the magnetization is 1). If the applied field begins increasing at this reversal field to obtain a FORC, then the $i=1$ hysteron switches positive at $H_a=h_1^c+J$ (where we have assumed that the switching of one pillar produces an infinitesimal change in M). The combination of these two switching events (a negative switch at $-h_1^c+J$ and a positive switch at h_1^c+J) contributes to the FORC distribution at $H_b=-J$ and $H_c=h_1^c$, which corresponds to the upper endpoint of the vertical distribution in Fig. 6(b).

Similarly, as the reversal field is lowered from saturation, the last hysteron to switch negative is $i=N$ at $H_r=-h_N^c-J$ (where the magnetization is near negative saturation when the last hysteron switches negative). If the applied field begins increasing at this reversal field, then the $i=1$ hysteron is the first to switch positive at $H_a=h_1^c+J$. But since the coercivity distribution is narrow, then to a good approximation we can approximate this pair of negative and positive switching fields as $H_r=-\langle h_c\rangle-J$ and $H_a=\langle h_c\rangle-J$, respectively. This pair of switching events contributes to the FORC distribution in H_c,H_b coordinates at $H_c=\langle h_c\rangle$ and $H_b=-J$. This corresponds to the lower endpoint of the vertical distribution in

Fig. 6(b). Hence, we have an understanding of the location of the two endpoints of the vertically elongated distribution in Fig. 6(b).

We next consider a system of hysterons with a broader coercivity distribution. We will use a gamma distribution of coercivities[21] of the form

$$f(h_c) = b^{-a} e^{-h_c/b} h_c^{(-1+a)} / \Gamma(a). \tag{9}$$

In this paper, we will let $a = 10.1$ mT and $b = 2.97$ [which has a peak at $(a-1)b = 27$ mT]. The motivation for these numerical values of a and b is that, as shown below, they give us a good fit to the experimental data in Fig. 5(b). The FORCs were numerically calculated with $J = 0$, as shown in Fig. 6(c). The resulting FORC distribution in Fig. 6(d) consists of a horizontal ridge on the $H_b = 0$ axis. If the field spacings of this dataset were made finer, this ridge would approach the form $\delta(H_b) f(H_c)$ (as mentioned in Sec. II). When the interaction strength is increased to $J = 21.1$ mT in Figs. 6(e) and 6(f), the FORC distribution forms a wishbone structure similar to that in the experimental data of Fig. 5(b). A negative region can be seen just below the $H_b = 0$ axis at high coercivity. A similar negative region is seen in the experimental data.

To summarize our numerical results so far, a collection of symmetric hysterons with distributed coercivities with a simple antiparallel mean interaction field generates a FORC distribution with the same basic "wishbone" signature as our nanopillar array sample. The remainder of this paper refines this basic result by, first, introducing more realistic "dipolar" interactions; second, putting disorder into the interactions; and, third, employing curvilinear hysterons.

Before doing that, however, we suggest the following qualitative explanation for the upper branch of the wishbone pattern in Fig. 6(f). Let us refer to FORCs which have reversal points near positive saturation as "upper" FORCs. Similarly, we will refer to the FORCs which start from near negative saturation as "lower" FORCs. On the upper FORCs, the last hysterons to switch positive are low coercivity hysterons. But, on the lower FORCs, the last hysterons to switch positive are high coercivity hysterons. Thus, the applied field necessary to return the system to positive saturation becomes larger as the reversal field is lowered. This effect can be seen in the FORCs of Fig. 6(e). The point where the FORCs return to positive saturation is "pushed" out to higher fields as the reversal field is lowered. This is qualitatively the cause of the upper branch of the wishbone in Fig. 6(f).

V. DIPOLAR INTERACTIONS

Looking at the experimental FORC diagram in Fig. 5(b), it can be seen that the upper branch has two distinct peaks. We next show that this two-peak structure arises when we consider non-mean-field forms for the interactions.

Let us consider a 2-D square array of hysterons with a uniform coupling in a local neighborhood about each pillar. This local neighborhood consists of nearest and next-nearest neighbors, i.e., a 3×3 square about each pillar. The interaction field at the ith particle becomes

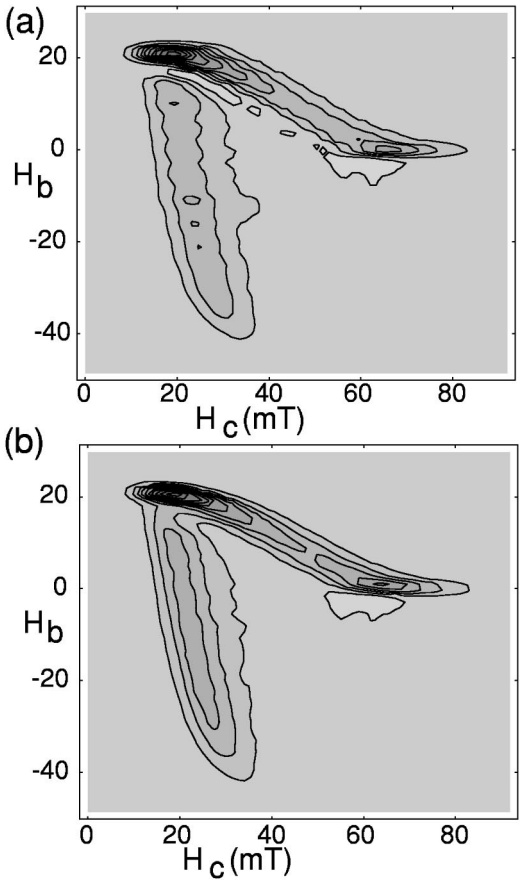

FIG. 7. The calculated FORC distribution of a 2-D array of hysterons with gamma distribution of coercivities and local antiparallel interactions ($J = 21.1$ mT). Two types of interactions were used. In (a), a 3×3 local interaction neighborhood with uniform coupling [see Eq. (10)]. In (b), "dipolar" interactions with a 11×11 interaction neighborhood [see Eq. (11)].

$$H_i^{int} = -\frac{J}{8} \sum_{3\times 3} s_j, \tag{10}$$

where this sum does not include the ith pillar itself. The factor of 8 in the denominator is chosen because each hysteron interacts with eight neighbors. It is the analog of the $1/N$ in Eq. (5) in the mean field interaction case. We calculated the FORC distribution with a grid of size 400×400 and with $J = 21.1$ mT. As seen in Fig. 7(a), the resulting distribution now has two distinct peaks: one prominent peak in the upper left of the diagram and another weaker peak at high coercivity on the $H_b = 0$ axis. We next suggest explanations for these two peaks, starting with the upper left peak.

As the reversal field is lowered from positive saturation, those hysterons which switch negative at the upper reversal fields (i.e., near positive saturation) will be dispersed through the system. Because of the locality of the interaction field in Eq. (10), these hysterons will seldom interact with one another. Hence, they will all see the same interaction field when they switch negative. When these hysterons switch back to positive on the upper FORCs they will still see this same interaction field. Hence, those hysterons which switch

negative at an upper reversal fields will all have the same bias; they will also generally be low coercivity hysterons. The result is a horizontal ridge at $H_b = J$ and small H_c.

The high coercivity peak in Fig. 7(a) can be explained by the "completion symmetry" described in Sec. II. We propose that a certain fraction of the pillars in this sample consistently are the last pillars in their local neighborhoods to switch into the direction of the applied field. As discussed in Sec. II, the interactions will not give any bias to these "completion pillars". This, we suggest, accounts for the high coercivity peak on the H_c (i.e., zero bias) axis in Fig. 7(a).

We consider next interactions with a $1/r^3$ dependence, which we will refer to as "dipolar" interactions. In order to make our numerical calculations practical, we have restricted this interaction to a local 11×11 neighborhood centered around each hysteron. The interaction field is written as

$$H_i^{int} = -J \sum_{11\times 11} \frac{s_j}{r_{ij}^3} \Bigg/ \sum_{11\times 11} r_{ij}^3, \tag{11}$$

where r_{ij} is the distance between the i and j hysterons, and where this sum does not include the ith pillar itself. We calculated the FORC distribution using Eq. (11) and again with $J = 21.1$ mT. It can be seen in Fig. 7(b) that with a $1/r^3$ interaction this model behaves much as it did with the uniform next-nearest neighbor interaction in Fig. 7(a).

VI. DISORDER

In the modeling results so far, we have shown that the wishbone structure seen in experiment can be accounted for with a simple mean field model and with distributed hysteron coercivities. When the mean field is replaced with dipolar interactions, the upper branch of the wishbone develops two distinct peaks at opposite ends. However, the magnitude of the upper peak is much more pronounced in the calculated FORC diagram [Fig. 7(b)] than in the experimental result [Fig. 5(b)]. As we show next, when disorder is introduced into the interactions, this peak is smoothed and its magnitude is reduced.

To justify the introduction of disorder, we note that the pillars in the array do not have precisely uniform size or shape, and that since each pillar contains a number of nickel grains, their microstructure is nonuniform. Hence, the coupling between pillars will not be perfectly described by a dipolar $1/r^3$ expression. Therefore, let us introduce disorder into the interactions by writing

$$H_i^{int} = -J \sum_{11\times 11} \frac{(1 + \sigma_J R_{ij}) s_j}{r_{ij}^3} \Bigg/ \sum_{11\times 11} r^3, \tag{12}$$

where R_i is a normally distributed random number with standard deviation 1 and mean zero (R_{ij} is fixed for a given i and j). The degree of disorder in Eq. (12) is governed by σ_J. We calculated the FORC distribution with $\sigma_J = 0.35$ and again with $J = 21.1$ mT. As seen in Fig. 8(a), the magnitude of the upper peak on the upper branch has been reduced, and is now in better agreement with the experimental data.

However, with the upper peak reduced, we can now see that the high coercivity peak in Fig. 8(a) is too large. This is due to the fact that the completion symmetry discussed earlier remains intact even with the disorder in Eq. (12). To reduce the high coercivity peak, we must break this completion symmetry. One possible physical mechanism that would accomplish this is a random bias field. A random bias field could arise if some spins of the system are frozen into specific directions at the energy and time scales considered here. Such freezing might arise from high local crystalline or shape anisotropies, and would give rise to an effective random bias field.

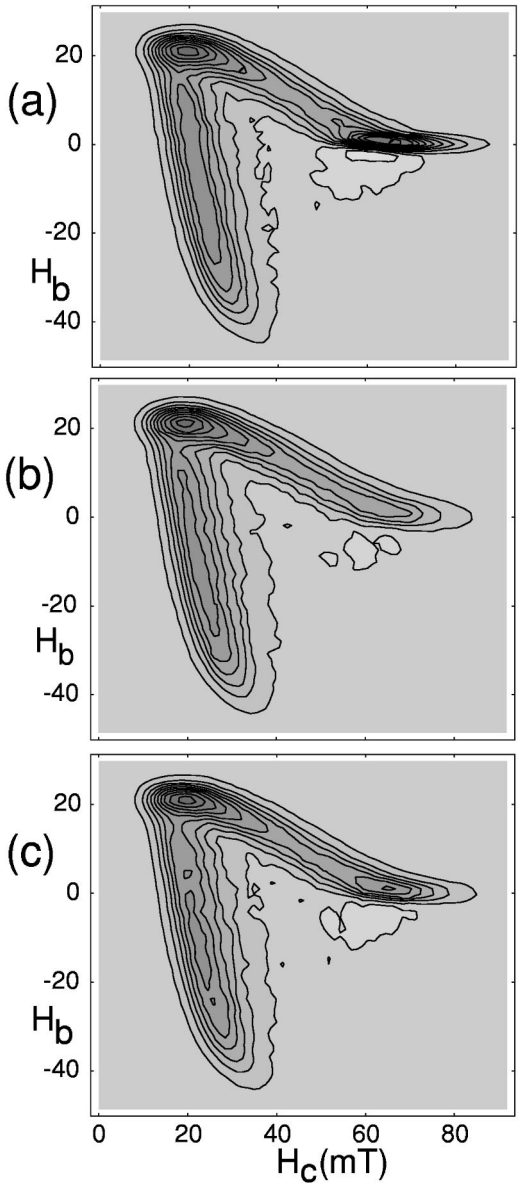

FIG. 8. The calculated FORC distribution with "dipolar" interactions and disorder. A gamma distribution of coercivities is used and $J = 21.1$ mT. In (a), a random term is inserted into the coupling with $\sigma_j = 0.35$ [see Eq. (12)]. In (b), a random bias field is inserted at each hysteron site with $\sigma_b = 0.076$ [see Eq. (13)]. In (c), a random bias field and a random term in the coupling are combined, with $\sigma_b = 0.049$ and $\sigma_j = 0.24$ [see Eq. (14)].

We can rewrite the interaction field with a random bias field as

$$H_i^{int} = -J\left(\sigma_b R_i + \sum_{11\times 11} \frac{s_j}{r_{ij}^3} \Big/ \sum_{11\times 11} r^3\right), \tag{13}$$

where σ_b governs the degree of disorder (R_i is fixed for a given i). When we recalculate the FORC distribution with $\sigma_b = 0.076$ and $J = 21.1$ mT, as seen in Fig. 8(b), the high coercivity peak is gone. Hence, only a small random bias field is required to achieve the desired result.

Finally, we combine these two types of disorder,

$$H_i^{int} = -J\left(\sigma_b R_i + \sum_{11\times 11} \frac{(1+\sigma_J R_{ij}) s_j}{r_{ij}^3} \Big/ \sum_{11\times 11} r^3\right), \tag{14}$$

and we recalculate the FORC distribution with $\sigma_b = 0.049$, $\sigma_J = 0.24$, and $J = 21.1$ mT, as seen in Fig. 8(c). With this combination of disorder, the magnitudes of the two peaks on the upper branch occur in approximate agreement with the experimental data of Fig. 5(b).

VII. CURVILINEAR HYSTERONS

The nickel pillars in our sample are oriented perpendicular to the substrate and aligned with the applied field. If they behaved as Stoner-Wohlfarth particles, then they would have no reversible magnetization. But micromagnetic calculations show that nickel pillars of the size in our sample have "flower" remanent states, and that their remanent magnetization measured in units of the saturation magnetization is less than 1.[7] This indicates that these pillars have some reversible magnetization. Furthermore, the experimental FORC distribution in Fig. 5(b) exhibits a substantial reversible ridge. Therefore, we next incorporate a reversible magnetization into our model by replacing the square hysterons with curvilinear hysterons. Curvilinear hysterons have been previously used in Refs. 22 and 23.

The magnetization of a curvilinear hysteron with coercivity h_c can be represented as $s^{cl}[s,H,h_c]$, where H is the applied field and $s = \pm 1$ is the state of a symmetric square hysteron with the same coercivity h_c. For our numerical calculations, we require a functional form for $s^{cl}[s,H,h_c]$. However, the magnetic reversal of these pillars is sensitive to irregularities in their shape, to crystalline imperfections and surface roughness, and to oxidation state. All these factors make an analytical or numerical solution for the hysteresis of these pillars problematic. Therefore, we have used a phenomenological functional form for our curvilinear hysterons which results in good agreement between experiment and data. This functional form is

$$\begin{aligned} s^{cl}[s,H,h_c] \equiv s + (1 - \mathrm{Tanh}(0.106 h_c - 4))^{\frac{1}{2}} \\ \times \{0.18[\mathrm{Tanh}(H/35.1) - s] \\ - s 0.375\ \mathrm{Max}[0,(27.0 - sH)/(27.0 + h_c)]^{3.6}\}. \end{aligned} \tag{15}$$

This functional form has two notable properties which we have found improve the agreement to data: First, the factor $[1-\mathrm{Tanh}(0.106h_c-4)]$ forces the size of the reversible component to decrease with increasing h_c. Second, the term containing "Max" results in a rapidly increasing curvature as the discontinuous jump is approached. These two properties can be seen in Fig. 9(a), where we plot curvilinear hysterons of this functional form for several values of h_c, and where these hysterons are superimposed on the gamma distribution of h_c described earlier.

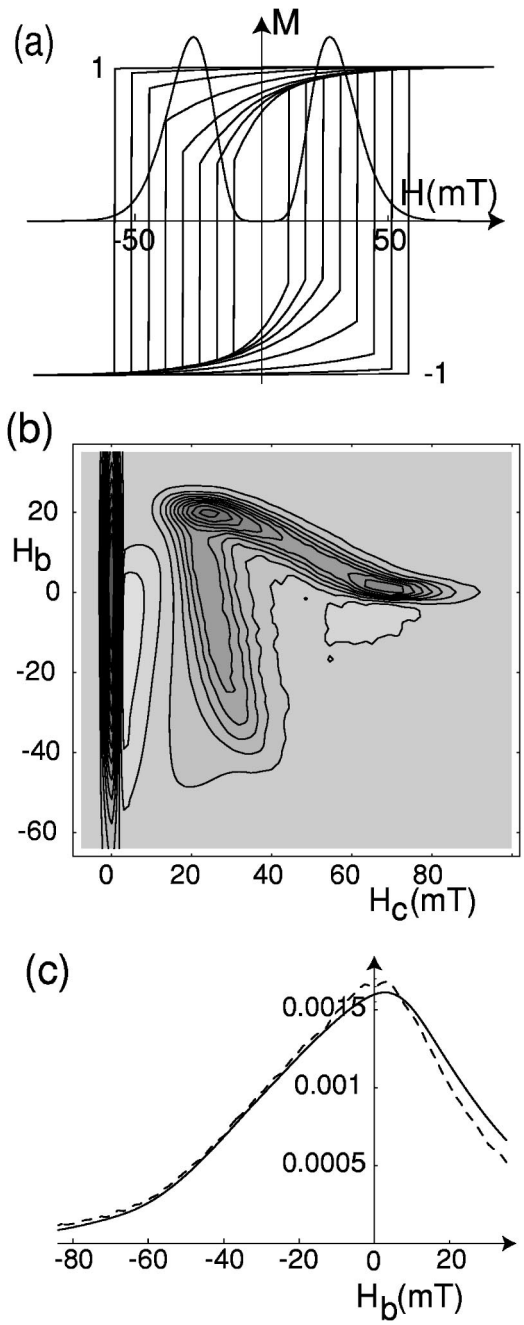

FIG. 9. (a) The curvilinear hysterons superimposed upon the distribution of coercivities. (b) The numerically calculated FORC distributions with "dipole" interactions and curvilinear hysterons. (c) The vertical cross section through the reversible ridge of the FORC distributions at $H_c = 0$. The dotted line is from the experimental data in Fig. 5(c) for comparison.

With curvilinear hysterons, the total magnetization of an interacting system becomes

$$M = \sum_i s^{\mathrm{cl}}[s_i, H + H_i^{int}, h_i^c]/N, \tag{16}$$

and the interaction field in Eq. (14) becomes

$$H_i^{int} = -J\sigma_b R_i - J \sum_{11\times 11} \frac{(1+\sigma_J R_{ij}) s^{\mathrm{cl}}[s_j, H + H_j^{int}, h_j^c]}{r_{ij}^3} \Bigg/ \sum_{11\times 11} r^3. \tag{17}$$

In our algorithm, the state of the square hysteron s_i is updated at a given field using the coercivity h_i^c, the applied field H, and the interaction field H_i^{int}, which is evaluated using the state of the system at the previous field step. Then the value of the ith curvilinear hysteron is calculated using Eq. (15) as a function of this updated s_i, and also as a function of H, h_i^c, and H_i^{int} (where the latter is evaluated at the previous field step).

A set of FORCs was calculated with the "dipolar" interactions in Eq. (17) and with $a=10.1$, $b=2.97$, $J=25.5$, $\sigma_b=0.049$, and $\sigma_J=0.24$. The resulting FORC distribution, shown in Fig. 9(b), has a prominent reversible ridge. The field spacing of our calculated FORC dataset is $H_{\mathrm{sp}}=1.5$ mT, which is the same as that of the experimental data in Fig. 5. This allows us to make a quantitative comparison between our calculated reversible ridge and the experimentally measured reversible ridge in Fig. 5(b). In Fig. 9(c), it can be seen that vertical cross sections at $H_c=0$ through the calculated and experimental reversible ridges are in good agreement. Finally, a negative valley can be seen just to the right of the reversible ridge. This is also in agreement with the experimental data in Fig. 5(b). This negative valley has the same basic explanation as the negative valley in Fig. 3(b). It can be attributed to the fact that the slope (or susceptibility) of our curvilinear hysterons near their negative switching field is greater on the top branch than on the bottom.

VIII. CHOICE OF MODEL PARAMETERS

These parameter values for our final FORC diagram in Fig. 9(b) were selected by optimizing the agreement between data and experiment one parameter at a time. The results of a given optimization in one parameter were used as the initial condition for the next optimization in another parameter, and this process was carried out repeatedly over many iterations over all the parameters. We suggest that this procedure brings us reasonably close to an optimal fit. In Fig. 10(a) we have overlaid this final result upon the experimental FORC distribution in Fig. 5(b). The contour shading in Fig. 10(a) has been omitted, and the contour lines of the experimental diagram are widened and lightened, to help distinguish the two distributions. There appears to be good agreement between modeling and experiment.

It may be instructive to consider what changes occur in the FORC distribution when we modify our final result by using a more narrow Gamma distribution. We changed a (from 10.1) to 19.0 mT and b (from 2.97) to 1.47, which changes the standard deviation from 9.4201 to 6.40758 mT

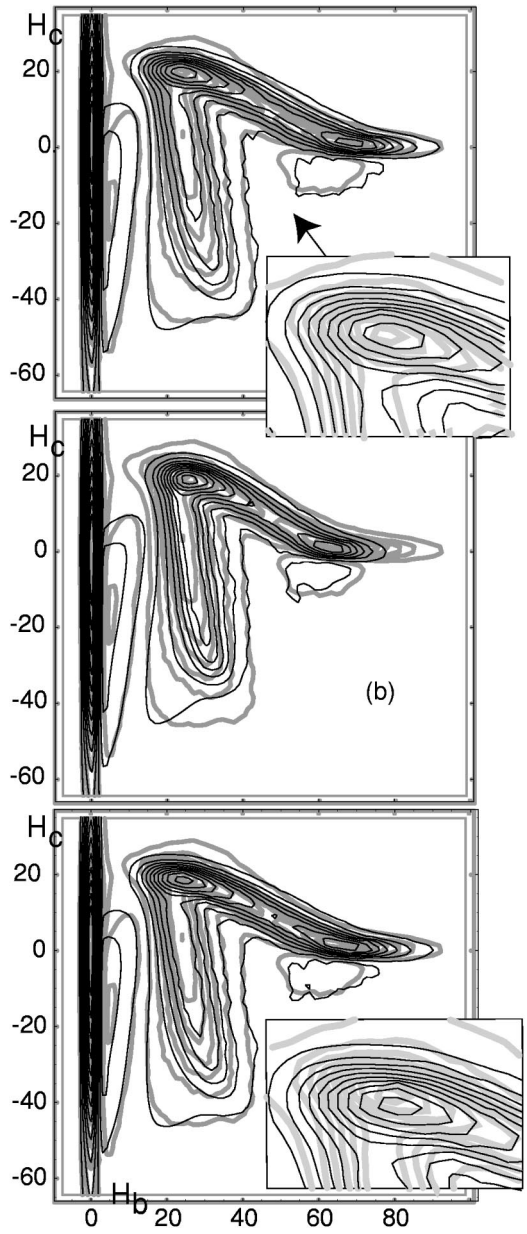

FIG. 10. The overlay of modeled and experimental FORC distributions. The contour lines of the experimental result are widened and lightened (a) with "optimal" parameters, (b) with a broader distribution of coercivities, and (c) with decreased coupling strength. The insets are to emphasize that the decreased coupling lowers the vertical location of the upper peak.

but leaves the peak location unchanged. The modified result is overlaid on the experimental data in Fig. 10(b). It can be seen on the right-hand side of the diagram that the modified distribution does not reach as high a coercivity as it should.

Similarly, we recalculated the FORC distribution after increasing J from 25.5 to 23.8 mT. The modified result is overlaid on the experimental result in Fig. 10(c). It can be seen that the top peak of the modified FORC distribution is significantly lower than that of the experiment. We note that the discrepancies produced by changing J and a in Fig. 10 appear to be distinct and somewhat "orthogonal." These re-

sults help us have confidence that our final parameter values are reasonably close to optimal values.

IX. DISCUSSION

The modeling work in this paper is an extension of earlier work in Refs. 24 and 7. In this work, a pillar array sample like the one studied here was represented by a 12×12 array of square hysterons, with a Gaussian distribution of coercivities. The mean of this Gaussian coercivity distribution was set equal to the measured coercivity of the major hysteresis loop. The antiparallel couplings between the hysterons were calculated from the measured physical dimensions of the pillar array (i.e., pillar height, diameter, spacing, and spontaneous magnetization). And, finally, the standard deviation of the coercivity distribution, in this earlier work, was adjusted in order to fit the calculated major hysteresis loop with the measured loop.

In this paper, we have augmented this earlier modeling by employing curvilinear hysterons and incorporating disorder into the interactions. We also made the mean of our coercivity distribution a fitting parameter. As a result, our modeling has several more fitting parameters than the modeling described just above.[7,24] However, the FORC distribution contains more information than does the major hysteresis loop, and so, at least in principle, we should be able to fit more parameters.

The interaction parameter J in this paper is the interaction field seen by the pillars in a saturated state. A good fit of modeling to data was achieved with $J=25.5$ mT. We can also calculate J from the measured parameters of the sample. The pillars are 250 nm in height, but have rounded tops, so we will approximate the height as 210 nm. Their diameter is 92 nm, spacing is 200 nm, and the size of sample is 0.0665 cm^2. The saturation magnetization is 49.4×10^{-6} emu (this was actually measured parallel to the plane of the substrate because there appear to be problems in calibrating the instrument in the perpendicular direction). This gives a spontaneous magnetization for the nickel of $M_{sp} = 213$ emu/cc or 21.3 mT (this is lower than the value of 320 emu/cc given in Ref. 7 for a similar sample, which may be a result of oxidation of these Ni pillars during storage in atmosphere). The dipolar field between nearest neighbors in the saturated state is obtained by multiplying M_{sp} by pillar volume and dividing by distance cubed, which gives 3.71 mT for nearest neighbors. In a square array, the total dipole field is nine times the dipole field from a nearest neighbor[24] which gives an interaction field of 33.4 mT. For closely spaced particles, the dipole approximation can overestimate the interaction field by as much as 17.4%.[24,25] This gives a dipole interaction field in the saturated state of 27.7 mT. Hence, the J obtained by fitting our model to data in consistent with that calculated from the physical dimensions and saturation magnetization of the sample.

X. CONCLUSION

In this paper we report the FORC diagram signature of a perpendicular nickel nanopillar array. The dominant feature of this FORC distribution is a two-branch "wishbone" structure. We showed that this wishbone signature can be accounted for by a simple model consisting of symmetric hysterons with distributed coercivities and a negative (antiparallel) mean field interaction. In this modeling, we find that the extent of vertical spread of the FORC distribution is a measure of the interaction strength.

In addition to the wishbone structure, the FORC diagram signature of our pillar sample has several finer features. There is, first, a negative region at high coercivity just below the $H_b=0$ axis. This feature also comes out of our simple mean field calculation. Second, the upper branch of the wishbone contains two distinct peaks. These two peaks arise in our simple hysteron model when we replace the mean interaction field with a field having a $1/r^3$ dependence. We have referred to this as a "dipolar" interaction field. Introducing disorder into the interactions of our model has been shown to smooth these two peaks and reduce their magnitude, which improves the agreement with the measured FORC signature.

In addition to the wishbone structure, the FORC distribution also has a prominent reversible ridge, and negative region just adjacent this ridge. Both of these features can be produced in modeling through the use of curvilinear hysterons.

We recognize that the modeling performed here is phenomenological in nature. A more rigorous model based, for example, on the Landau-Lifshitz-Gilbert equations of micromagnetics, would be desirable. Interesting steps have been taken in this direction[26] but at present a rigorous model of an array of thousands of nickel pillars is not feasible. Therefore, we believe that simplified modeling such as the modeling done here can serve a useful purpose in understanding qualitatively how the features of a measured FORC signature relate to the physics of the system.

As perpendicular and patterned recording media are of increasing interest in research and industry, FORC diagrams may become a useful tool in the characterization of these media. This paper is a first step in making this possible, by providing a qualitative physical understanding of the FORC diagram signature of one perpendicular media. An obvious next step for future work is to collect the FORC diagrams of perpendicular arrays with varying pillar sizes, different spacing, and different materials.

ACKNOWLEDGMENTS

This work was supported by the University of California Office of the President through the Campus Laboratory Collaboration and Campus Laboratory Exchange programs. Simulations were performed on computers purchased through NSF-MRI-EAR-0216346. The authors wish to thank Dr. Kenneth Verosub for use of his AGM, and M. Farhoud for her work in sample preparation.

APPENDIX: MEAN FIELD, NARROW COERCIVITY DISTRIBUTION

Let $f(h_c)$ be an extremely narrow distribution with mean $\langle h_c \rangle$. As the reversal field is lowered from positive saturation, the magnetization satisfies this equation:

$$M = -\int_0^{\mathrm{Max}[0,-(H_r-JM)]} f(h_c)dh_c + \int_{\mathrm{Max}[0,-(H_r-JM)]}^{\infty} f(h_c)dh_c. \tag{A1}$$

Since $f(h_c)$ is very narrow, if M is between −1 and 1, then a solution to Eq. (A1) can only be obtained if $-(H-JM)$ is very close to $\langle h_c\rangle$. So, if $-1 \leqslant M \leqslant 1$, then we can write

$$-(H_r - JM) = \langle h_c\rangle. \tag{A2}$$

This implies that we can write $M(H_r)$ as

$$M(H_r) = \mathrm{Max}[-1, \mathrm{Min}[1, (\langle h_c\rangle + H_r)/J]]. \tag{A3}$$

Taking the derivative with respect to H_r we get

$$\frac{dM(H_r)}{dH_r} = \frac{1}{J}\theta(1 - (\langle h_c\rangle + H_r)/J)\,\theta((\langle h_c\rangle + H_r)/J + 1), \tag{A4}$$

where $\theta(x)$ is the "step" function, such that $\theta(x)$ equals 0 if $x<0$ and equals 1 if $x \geqslant 0$.

Similarly, on a FORC with reversal field H_r, as the applied field is increased

$$M = M(H_r) + 2\int_0^{\mathrm{Max}[0,\mathrm{Min}[-(H_r-JM_r),H_a-JM]]} f(h_c)dh_c. \tag{A5}$$

Since $f(h_c)$ is very narrow, if M is between $M(H_r)$ and 1, then a solution to Eq. (A5) can only be obtained if $-(H_a - JM)$ is very close to $\langle h_c\rangle$. So

$$M(H_r,H_a) = \mathrm{Min}[1, \mathrm{Max}[M(H_r), (H_a - \langle h_c\rangle)/J]]. \tag{A6}$$

Taking the derivative with respect to H_a, and using Eq. (A4) we get

$$\frac{\partial M(H_r,H_a)}{\partial H_a} = \frac{1}{J}\theta(1 - (H_a - \langle h_c\rangle)/J) \times \theta((H_a - \langle h_c\rangle)/J - M(H_r)). \tag{A7}$$

Taking the derivative with respect to H_r we get

$$\frac{\partial^2 M(H_r,H_a)}{\partial H_a \partial H_r} = \frac{-1}{J}\theta(1 - (H_a - \langle h_c\rangle)/J) \times \delta((H_a - \langle h_c\rangle)/J - M(H_r)) \times \frac{1}{J}\theta(1 - (\langle h_c\rangle + H_r)/J)\,\theta((\langle h_c\rangle + H_r)/J + 1). \tag{A8}$$

When $(H_r + \langle h_c\rangle)/J$ is greater than 1 or less than −1, the product of the step functions in Eq. (A8) equals zero. Therefore, the expression for $M(H_r)$ in Eq. (A3) can be replaced with $(H_r + \langle h_c\rangle)/J$ where $M(H_r)$ occurs in Eq. (A8). Equation (A8) becomes

$$\frac{\partial^2 M(H_r,H_a)}{\partial H_a \partial H_r} = \frac{-1}{J}\theta(1 - (H_a - \langle h_c\rangle)/J) \times \delta((H_a - \langle h_c\rangle)/J - (H_r + \langle h_c\rangle)/J) \times \frac{1}{J}\theta(1 - (\langle h_c\rangle + H_r)/J)\,\theta((\langle h_c\rangle + H_r)/J - 1). \tag{A9}$$

To convert the delta function to H_c, H_b coordinates we must divide by the Jacobian of the transformation, which is 1/2. So

$$\delta((H_a - \langle h_c\rangle)/J - (H_r + \langle h_c\rangle)/J)$$

in H_c, H_b coordinates becomes

$$2\delta((2H_c - 2\langle h_c\rangle)/J) = J\delta(H_c - \langle h_c\rangle).$$

Since this delta function is nonzero only at $H_c = \langle h_c\rangle$, then in the θ functions in Eq. (A9) we can make the replacements $H_r = H_b - \langle h_c\rangle$ and $H_a = H_b + \langle h_c\rangle$. We get

$$\frac{\partial^2 M(H_c,H_b)}{\partial H_c \partial H_b} = \frac{-1}{J}\theta(1 - H_b/J) \times \delta(H_c - \langle h_c\rangle)\,\theta(1 - H_b/J)\,\theta(H_b/J + 1). \tag{A10}$$

Note that one of the step functions in Eq. (A10) is redundant. The FORC distribution becomes

$$\rho(H_b,H_c) = -\frac{1}{2}\frac{\partial^2 M(H_c,H_b)}{\partial H_c \partial H_b} = \frac{1}{2J}\delta(H_c - \langle h_c\rangle)\,\theta(J - H_b)\,\theta(H_b + J). \tag{A11}$$

It can be seen that the total weight of this distribution is 1.

[1] C. A. Ross, Annu. Rev. Mater. Sci. **31**, 203 (2001).

[2] W. Wernsdorfer, E. B. Orozco, K. Hasselbach, A. Benoit, B. Barbara, N. Demoncy, A. Loiseau, H. Pascard, and D. Mailly, Phys. Rev. Lett. **78**, 1791 (1997).

[3] S. Wirth, M. Field, D. D. Awschalom, and S. von Molnar, Phys. Rev. B **57**, R14 028 (1998).

[4] R. P. Cowburn, D. K. Koltsov, A. O. Adeyeye, M. E. Welland, and D. M. Tricker, Phys. Rev. Lett. **83**, 1042 (1999).

[5] R. L. Stamps and R. E. Camley, Phys. Rev. B **60**, 11 694 (1999).
[6] K. Y. Guslienko, S. B. Choe, and S. C. Shin, Appl. Phys. Lett. **76**, 3609 (2000).
[7] C. A. Ross, M. Hwang, M. Shima, J. Y. Cheng, M. Farhoud, T. A. Savas, H. I. Smith, W. Schwarzacher, F. M. Ross, M. Redjdal, and F. B. Humphrey, Phys. Rev. B **65**, 144417 (2002).
[8] C. R. Pike, A. P. Roberts, and K. L. Verosub, J. Appl. Phys. **85**, 6660 (1999).
[9] I. D. Mayergoyz, IEEE Trans. Magn. **MAG-22**, 603 (1986).
[10] C. R. Pike and A. Fernandez, J. Appl. Phys. **85**, 6668 (1999).
[11] C. R. Pike, A. P. Roberts, and K. L. Verosub, Geophys. J. Int. **145**, 721 (2001).
[12] A. P. Roberts, C. R. Pike, and K. L. Verosub, J. Geophys. Res. **105**, 28461 (2001).
[13] C. R. Pike, A. P. Roberts, M. J. Dekkers, and K. L. Verosub, Phys. Earth Planet. Inter. **126**, 11 (2001).
[14] H. G. Katzgraber, F. Pazmandi, C. R. Pike, K. Liu, R. T. Scalettar, K. L. Verosub, and G. T. Zimanyi, Phys. Rev. Lett. **89**, 257202 (2002).
[15] A. R. Muxworthy and D. J. Dunlop, Earth Planet. Sci. Lett. **203**, 369 (2002).
[16] A. Stancu, C. R. Pike, L. Stoleriu, P. Postolache, and D. Cimpoesu, J. Appl. Phys. **93**, 6620 (2003).
[17] C. R. Pike, Phys. Rev. B **68**, 104424 (2003).
[18] R. Cammarano, P. McCormick, and R. Street, J. Phys. D **29**, 2327 (1996).
[19] C. R. Pike, R. T. Scalettar, and F. Pazmandi (unpublished).
[20] A. J. Newell, Geochem., Geophys., Geosyst. (to be published).
[21] A. Aharoni, *Introduction to the Theory of Ferromagnetism* (Clarendon Press, Oxford, 1996).
[22] E. Della Torre, *Magnetic Hysteresis* (IEEE Press, New York, 1999).
[23] I. D. Mayergoyz, *Mathematical Models of Hysteresis* (Springer-Verlag, New York, 1991).
[24] M. Hwang, M. C. Abraham, T. A. Savas, H. I. Smith, R. J. Ram, and C. A. Ross, J. Appl. Phys. **87**, 5108 (2000).
[25] M. Pardavi-Horvath and G. Zheng, IEEE Trans. Magn. **32**, 4469 (1996).
[26] G. Brown, M. A. Novotny, and P. A. Rikvold, Phys. Rev. B **64**, 134422 (2001).